Open Access

Recent Progress in Materials

LIDSEN Publishing Inc.

Research Article

Spark Plasma Sintering of Cu-Ti-Ni Ternary Alloy: Microstructural, Thermal and Electrical Properties

Amos O. Oyatogun [1, 2], Emmanuel Ajenifuja [1, 3, 4, *], Abimbola P. Popoola [1], Olawale Popoola [4], Fatai O. Aramide [1, 5], Grace M. Oyatogun [2]

1. Department of Chemical, Metallurgical and Materials Engineering, Tshwane University of Technology, Pretoria, South Africa; E-Mails: amosoyatogun1@gmail.com; eajenifuja@gmail.com; eajenifuja@oauife.edu.ng; popoolaapi@tut.ac.za; foaramide@futa.edu.ng
2. Department of Material Science and Engineering, Obafemi Awolowo University, Ile-Ife, Nigeria; E-Mail: oyatogun@oauife.edu.ng
3. Center for Energy Research and Development, Obafemi Awolowo University, Ile-Ife, Nigeria.
4. Centre for Energy and Electric Power, Tshwane University of Technology, Pretoria, South Africa; E-Mail: popoolao@tut.ac.za
5. Department of Metallurgical and Mat. Engineering, Federal University of Technology, Akure, Nigeria.

* **Correspondence:** Emmanuel Ajenifuja; E-Mails: eajenifuja@gmail.com; eajenifuja@oauife.edu.ng

Academic Editor: Ali Abdul-Aziz

Special Issue: Ceramic Matrix Composites: Performance Evaluation and Application

Recent Progress in Materials
2024, volume 6, issue 3
doi:10.21926/rpm.2403016

Received: December 28, 2023
Accepted: June 03, 2024
Published: July 01, 2024

Abstract

High strength and good conductivity are both critical parameters for copper-based alloys for electrical and other technological applications. This study is aimed to produce copper alloys and metal matrix composites (MMCs) with enhanced physical properties. Cu-Ti-Ni ternary alloys and MMCs samples were sintered at 600 to 700°C using spark plasma sintering (SPS), with a heating rate of 100°C/minutes, uniaxial pressure of 50 MPa, and a holding time of 10 minutes. Scanning electron microscopy (FE-SEM) was used to examine the microstructure,

while the relative densities of the composites were obtained via the Archimedes Principle method. A four-point probe and differential thermal analyzer (DTA) obtained electrical resistivity and thermal properties. The results indicated that the sample density nominally increases with sintering temperature but decreases with aluminium nitride additions. The electrical conductivity increases with the sintering temperature and AlN nanoparticle content. Distinct phase changes were observed from the DTA, occurring with the addition of AlN.

Keywords
Spark plasma sintering; Cu-Ti-Ni; AlN nanocomposites; densification; conductivity

1. Introduction

Copper-based alloys have been shown to possess good corrosion resistance, thermal conductivity, and electrical conductivity. Concerning the advancement of high-end technological industries, the demand and interest for these excellent properties of copper alloy have increased tremendously. Based on the previous, different copper-based metal matrix composite (MMCs) materials have evolved due to this demand [1-3]. Notably, the basic requirements for these copper group matrix composites are high strength and good conductivity [4-6]. Meanwhile, the alloys used for commercial electrodes are mainly CuCr, CuCrZr and BeCu. Copper-based electrodes need constant maintenance and frequent replacement, which decreases production efficiency and increases production costs. Therefore, the advancement of the copper metal matrix composite as electrode materials is of high importance [7, 8], and studies have shown that such composites can be prepared using various methods such as thermochemical [9, 10], in-situ synthesis [11], electro-metallurgical, cold deformation [12-14], and rapid condensation [15]. Most of these techniques are still at the initial stage and are far from the industrial-production level. Remarkably, the distribution of second-phase ceramic particles is not usually uniform within the matrix, and the requirement of high-temperature thermal stability is often difficult to attain. Meanwhile, powder metallurgy is a well-established formation process, and the distribution of second-phase reinforcement particles is comparatively uniform. If a proper optimization process is adopted, it can be used to prepare low-cost composites with improved mechanical and thermal properties.

Aluminium nitride (AlN) ceramic nanoparticle material is the most reasonable choice for matrix reinforcement without significantly reducing its electric conductivity. In recent times, the use of aluminium nitride has gained interest, and this is mainly because of its impressive attributes such as high thermal conductivity, good dielectric properties, high flexural strength, and high thermal expansion coefficient, which are all comparable to that of silicon [16]. AlN is stable in inert atmospheres at temperatures above 2000°C. These unique combinations of properties make aluminium nitride an advanced ceramic material for many future critical applications. Moreover, its non-toxic nature makes it a suitable alternative to beryllium [16-18]. Beryllium is widely applied in structural applications due to its low density, high flexural rigidity, thermal stability, and conductivity, making it a desirable aerospace material. However, it is a severe health and safety issue because exposure can lead to chronic diseases [19].

Meanwhile, studies have indicated that the addition of 2-5 wt. % AlN to copper increases its Brinell hardness and, subsequently, the strength of the resulting binary alloy [17]. For this study, aluminium nitride is considered the optimum choice for the Cu-Ti-Ni ternary matrix, and it is expected that its addition will significantly strengthen the composite and enhance its thermal stability while sustaining its electrical and thermal conductivity. In recent years, beryllium copper (Be-Cu) alloys have been considered the most viable for the design of high-temperature conducting devices. This is due to their strength, high thermal conductivity, and good mechanical properties at elevated temperatures. Their utilization was, however, limited by the health hazards associated with their production [19]. Hence, there is a need to investigate other copper-based systems as alternatives for the design of high-temperature conducting devices. Also, combining different vital properties in the same or single component is usually impossible with monolithic materials or alloys due to the trade-off effect [18, 19].

This study is conceptualized to adopt the spark plasma sintering technique to prepare the Cu-based MMCs with enhanced physical properties. The need to develop materials with novel internal structures and intricate geometries that traditional manufacturing cannot achieve has led to recent advancement. A typical example is the development of functionally graded materials (FGM), in which the material's properties are continuously graded along a specific direction via changes in composition and microstructure [20, 21]. The formation of diverse chemical compositions and the phase distribution of microstructure within a single material allow flexibility, and it represents a new research concept in the design of advanced engineering components [20, 21]. It will enable the ability to combine irreconcilable properties in the same components, which may not be possible with monolithic materials. Property distribution is needed in various typical products and applications with mutually exclusive requirements to provide multi-functional characteristics [20, 22-24]. The usual example of this phenomenon is found in the turbine blade, in which the blade core must be tough enough to withstand heavy dynamic loading. At the same time, its surface must have high thermal stability to withstand the high temperatures encountered during service [20, 21, 25]. Therefore, this study is methodized to enhance Cu-Ti-Ni ternary alloy's mechanical, electrical, and thermal stability by adding aluminium nitride ceramic using spark plasma sintering.

2. Methodology

2.1 Materials and Methods

Pure Cu powder (Centerline, Canada), Ti, Ni, and AlN powder (Sigma-Aldrich, Germany) were used as the constituents for the alloys, and their physical properties are given in Table 1. The powder mixtures were mild-milled using a tubular mixer (Tubular T2C Shaker-Mixer); added therein are 10 mm stainless steel balls as grinding media for uniform and optimal homogenization, mainly because of the ceramic AlN powder in the mixture. The ceramic AlN nanoparticle powder tends to agglomerate when exposed to air. The powder mixing was done under normal atmospheric conditions with a powder ratio (BPR) and milling time of 6:1 and 10 hours, respectively. The SPS machine (KCE-FCT-HHPD 25, Germany) used for sample preparation was set at the following operating parameters: vacuum pressure of 0.605 mbar (46.09%), relative pressure of 0.05 mbar, and absolute pressure of 1.2 mbar. The powder compaction was done using a sintering pressure of 50 MPa for all samples, while the isothermal temperature was varied from 600 to 700°C. Heating

rate and dwelling time of 100°C/m and 10 min were used, respectively. The sample dimension designed and obtained after sintering is 5 by 30 mm.

Table 1 Physical properties of the starting powders.

Powder	Particle size	Density (g/cm^3)	Purity (%)
Cu	40 µm	8.96	99.9
Ni	45-90 µm	8.91	99.9
Ti	45-90 µm	4.50	99.9
AlN	100 nm	3.26	99.5

2.2 Characterizations Details

The elemental and microstructural analysis of the composite and alloy samples was done using a field emission scanning electron microscope (FE-SEM) equipped with an EDX probe (Hitachi, SU8010). The densities of the specimen were measured after sintering using the Archimedes principle. In contrast, the relative densities were obtained by comparing the theoretical and actual densities before and after sintering. The SEM analysis was done with the following parameters: acceleration voltage of 20 kV, beam intensity of 14, and working distance of 15 mm, while the scan type is BSE. Analysis and characterization were done on metallographic samples prepared by grinding and polishing using SiC abrasive paper of grit size from P120 to P1200, with final polishing with the diamond solution. The images were taken on the etched samples after polishing. The etching was done with ferric chloride solution immersion for 15 minutes at room temperature (25°C). A differential thermal analyzer (DTA 404 Eos) was utilized for the thermal analysis. A sample mass of 5 mg was used for the DTA, and the experiment was carried out under normal atmospheric conditions. The temperature steps are as follows: Start at 30°C, Stop at 1200°C. The heating and data acquisition rates are 20 K/min and 100 pts/min, respectively. A four-point probe and electrical conductivity tester (HP2662, China) were used for the alloy samples. The current source was set at 100 mA and a speed of seven times/min. The conductivity test sample had a length of 20 mm × 20 mm and a thickness of 1.5 mm. The resistivity values obtained were converted to conductivities by using the inverse data.

3. Results and Discussions

3.1 Densification Properties

Compaction was performed on the mild-milled Cu-based alloy and composite powders using spark plasma sintering. The sintering, composition and densification parameters are presented in Table 2. The variation of the measured relative density (%ρ_{rel}) is observed to vary with composition and temperature, and it is shown that the relative density increases monotonously with sintering temperature. Increased relative density indicates suppressed porosity brought about by increasing sintering temperature. Yang and Conrad [26, 27] found a simultaneous increase in densification rates and reduced final grain sizes in yttria-stabilized zirconia samples prepared using SPS. The grain growth suppression requires an applied electric field in direct electrical contact with the consolidated powder sample, producing Joule heating via the electric current across the grain

interfaces [26]. It should be noted that the previous is mostly achievable in the spark plasma sintering process partly because of lower procedural duration. However, the relative density of the specimens containing AlN ceramic reinforcement appears lower than those of pure metal alloys.

Meanwhile, a maximum relative density value of 98.62% was obtained for the Cu-based alloys at 700°C. Therefore, using optimised processing conditions, it is possible to sinter the AlN-reinforced metal matrix composites with enhanced physical properties. The theoretical density is calculated using the following equation.

$$\frac{1}{\rho_{th}} = \left[\frac{M_{Cu}}{\rho_{Cu}} + \frac{M_{Ti}}{\rho_{Ti}} + \frac{M_{Ni}}{\rho_{Ni}}\right]\frac{1}{100} \quad (1)$$

Where ρ_{th} is theoretical density, while ρ and M are the normal density and wt.%, respectively.

Table 2 Compositions and densification properties of sintered samples.

Sample	Composition (wt. %)	Th. density (ρ_{th})	ST (°C)	Rel. Density (%ρ_{rel})
CTN-600	Cu12Ti12Ni	8.01	600	94.63
CTNA-600	Cu12Ti12Ni-1AlN	7.88	600	88.96
CTN-650	Cu12Ti12Ni	8.01	650	95.59
CTNA-650	Cu12Ti12Ni-1AlN	7.88	650	91.24
CTN-700	Cu12Ti12Ni	8.01	700	98.62
CTNA-700	Cu12Ti12Ni-1AlN	7.88	700	95.58

3.2 Microstructural Analysis

The micrographs from the SEM characterization of the Cu alloys and metal matrix composite (MMC) samples are shown in Figures 1-3 below. The morphological variations concern the sample compositions and sintering temperatures. Figure 1(a) shows that the microstructure has poor compactness with uneven particle distribution. In contrast, for the metal matrix composite (Figure 1b) with AlN addition, the microstructures show block structure with more distinct boundaries between phases. The ceramic intercalation promotes reactions between powder constituents, as shown in Figure 1(b). However, in other samples sintered at much higher temperatures (Figure 2b and Figure 3b), the metallurgical structure has even compactness. Therefore, it shows that with the increase in sintering temperature, the sintered body becomes more condensed with higher relative compaction. Notably, all the samples were prepared under the same uniaxial pressure condition, which generally benefits the samples' strength. It is noted in the samples that neither ceramic addition nor sintering temperature has a negligible effect on the uniformity of the grain sizes, as seen from the micrographs. The elemental composition of the circled phases common to all samples is shown in Figures 4-6. EDX analysis of the sites indicates that three main phases constitute the microstructures. These are mainly Cu-rich and Ti-rich phases distributed uniformly within each microstructure. Most of the ternary phases found at relatively higher temperatures (>800°C) do not appear to exist at 600°C, and the ternary intermediate phase Δ phase (CuNiTi) is restricted to 600°C [24]. However, based on the detailed EDX analysis of the samples, some ternary phases are observed to have formed with intermediate phases of the CuTi, NiTi, and Ni_3Ti, which are found to be peculiar to all samples. The corresponding representative EDX spectra for the observed phases, light-grey

Cu-rich (A), dark grey Ti-rich (B) and black Cu-rich (C), are shown in Figures 4-6. In contrast, the EDX spectrum for phases containing AlN constituent in the alloy microstructure is presented in Figure 7.

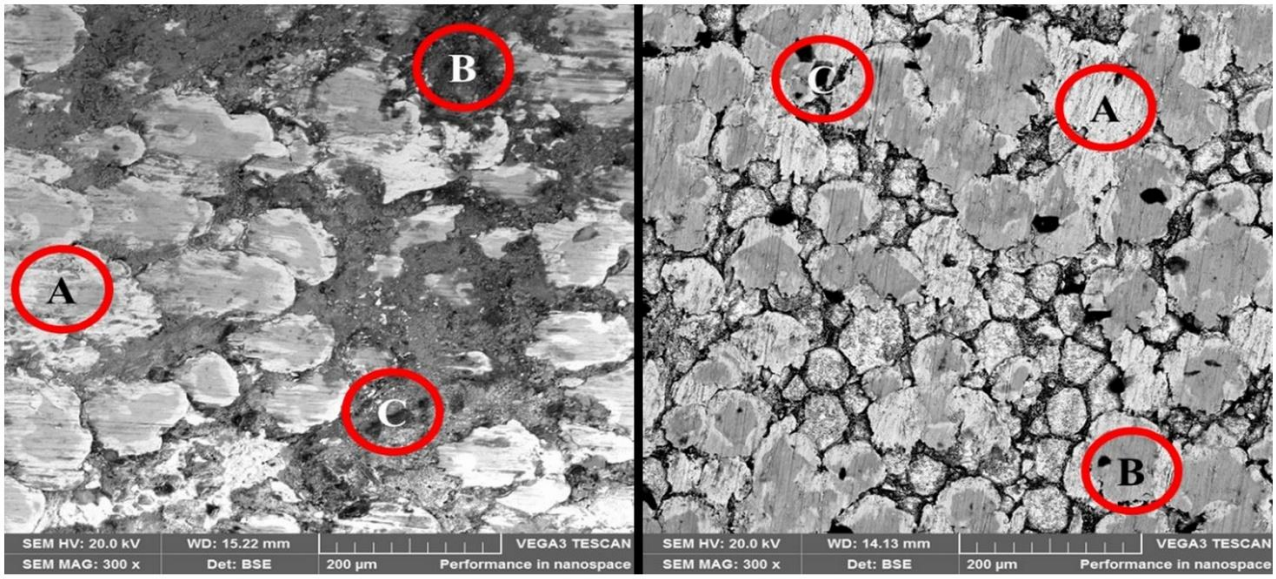

a) Sample CTN - 600 b) Sample CTNA - 600

Figure 1 SEM micrographs for Cu MMCs at 600°C.

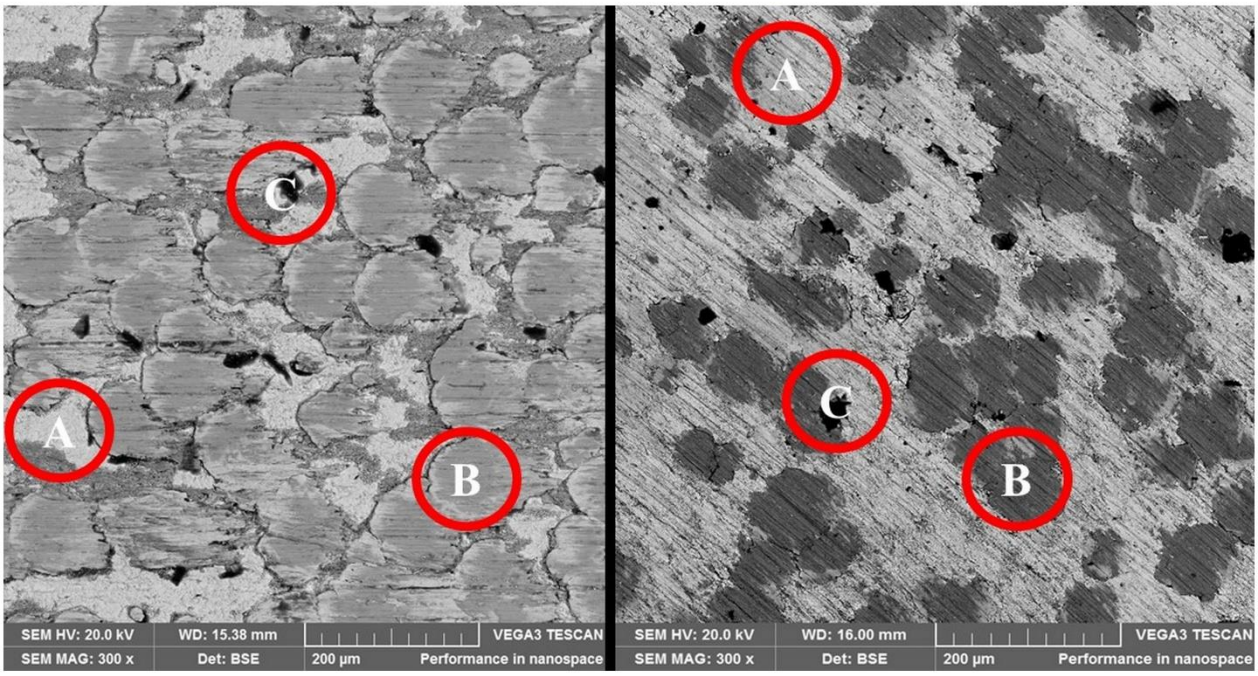

a) Sample CTN - 650 b) Sample CTNA - 650

Figure 2 SEM micrographs for Cu MMCs at 650°C.

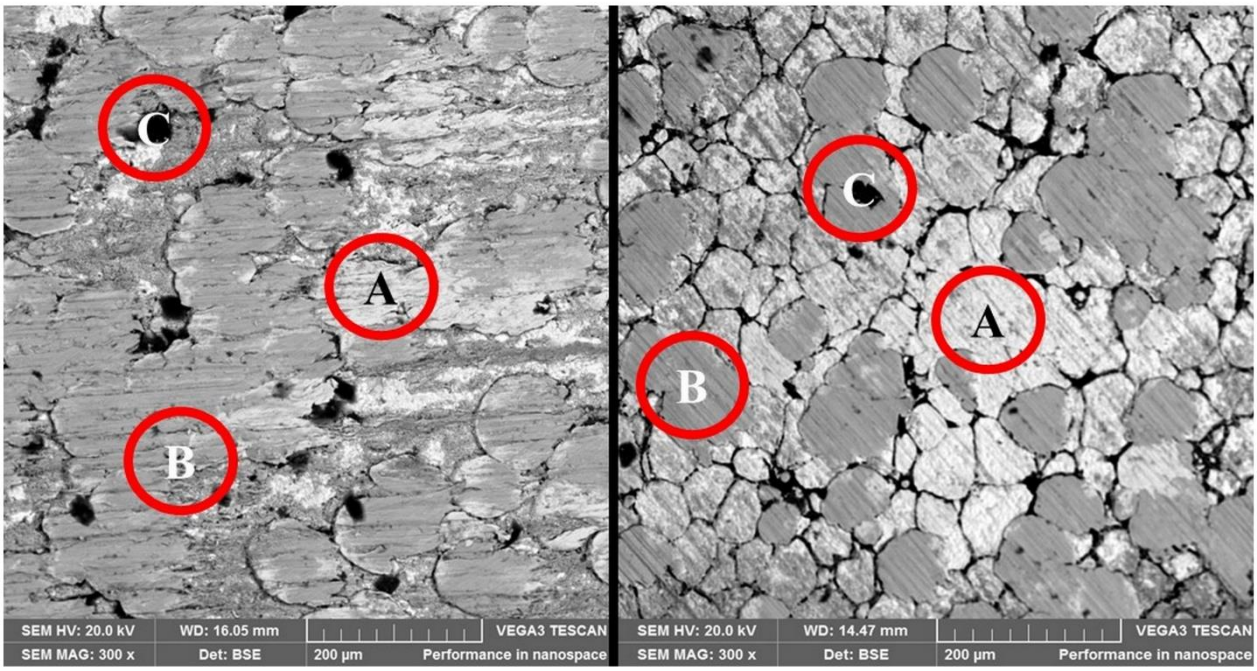

Figure 3 SEM micrographs for Cu MMCs at 700°C.

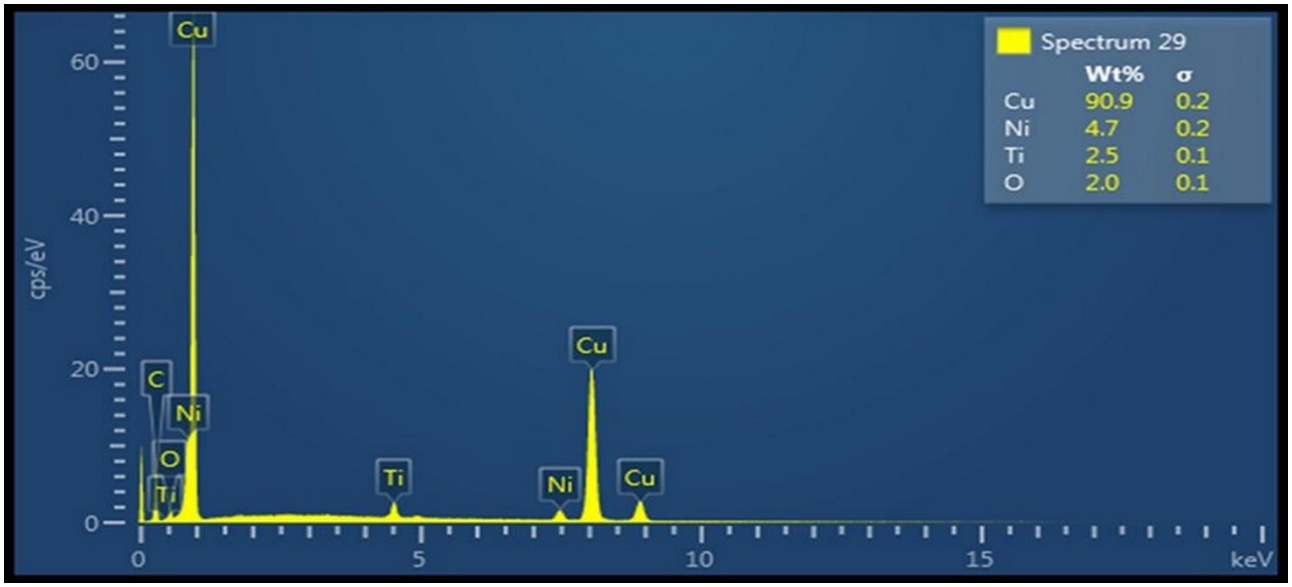

Figure 4 Representative EDX spectrum for light grey Cu-phase (A).

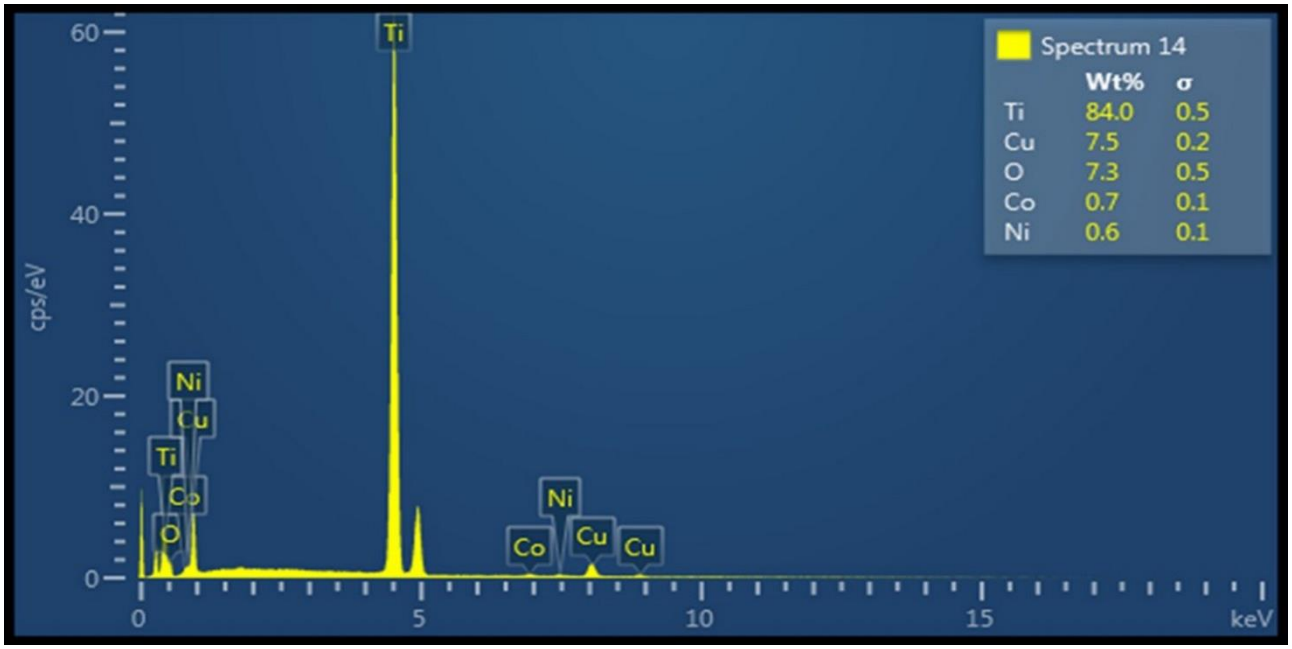

Figure 5 Representative EDX spectrum for dark grey Ti-rich phase (B).

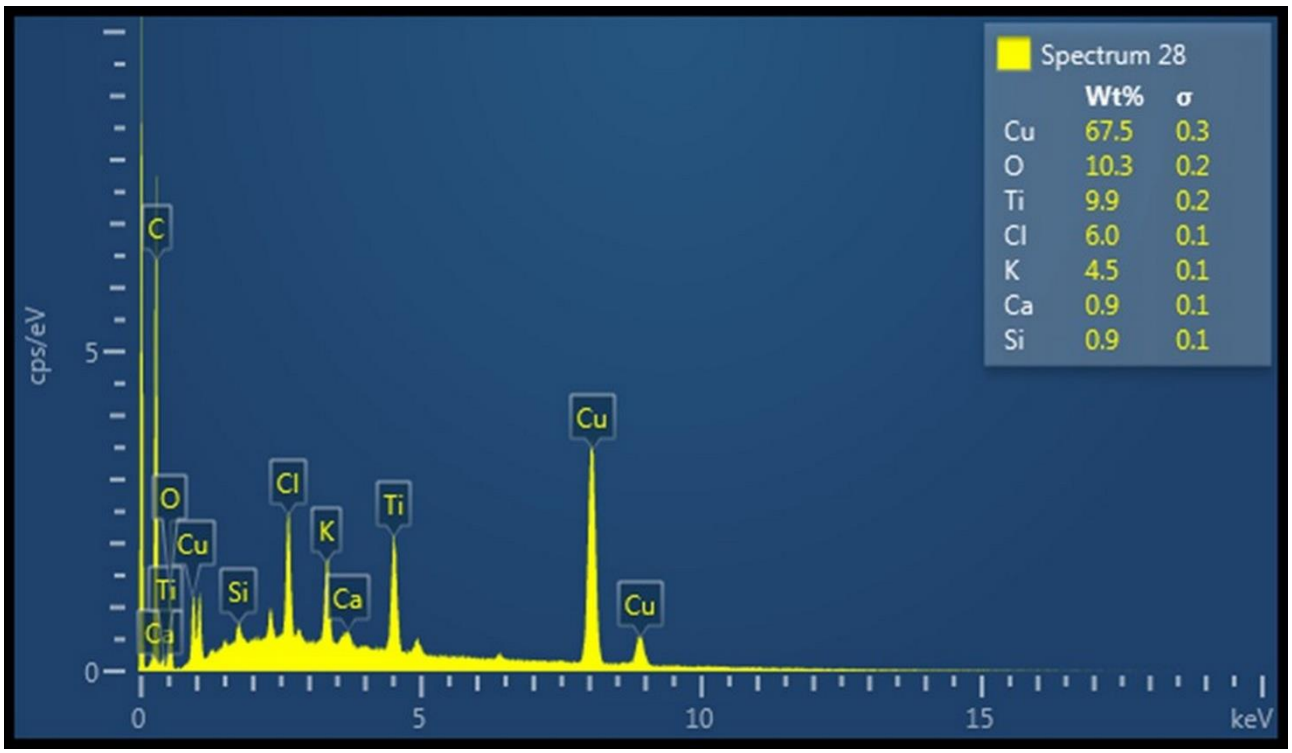

Figure 6 Represents the EDX spectrum for the black Cu-rich phase (C).

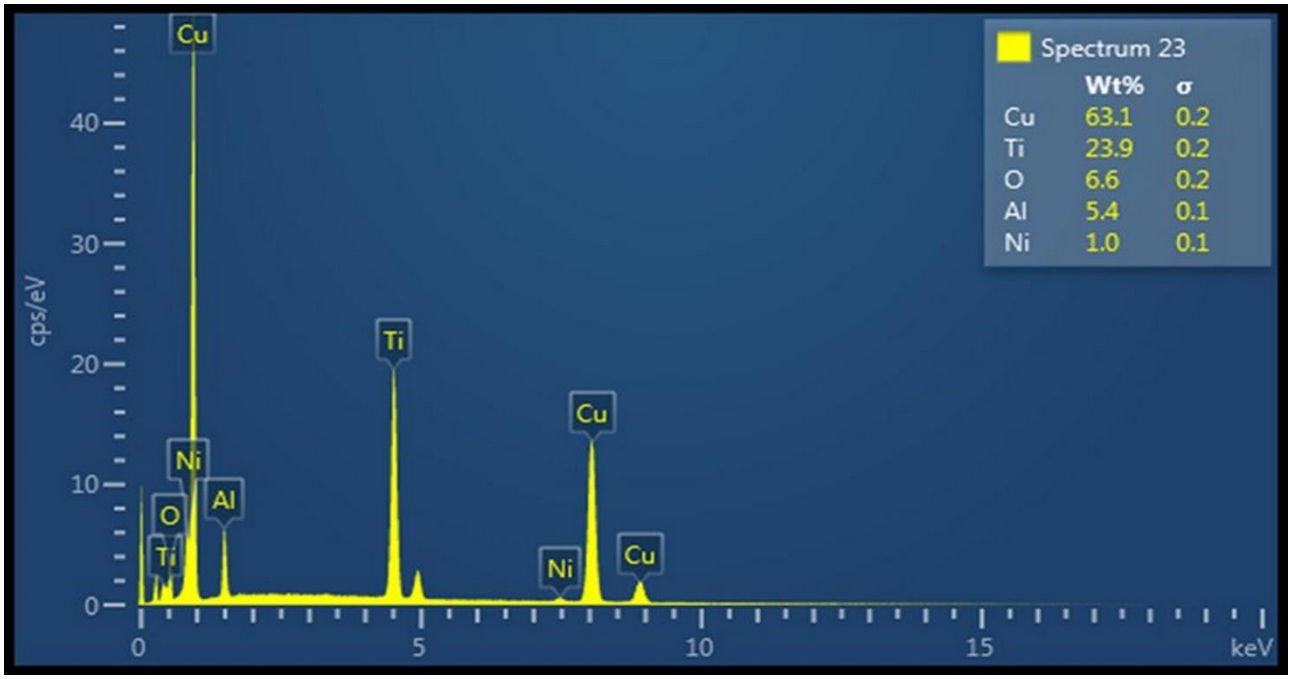

Figure 7 Represents the EDX spectrum for the black Cu-rich phase with Al content.

3.3 Thermal Properties

The thermograms for the alloy samples are shown in Figure 8. For alloy CTNA-600 with 1 wt.% of aluminium nitride, a broad endothermic peak is shown at 213.5°C, followed by two broad exothermic peaks at 494 and 631.6°C, respectively. These peaks are due to metal components and aluminium nitride reactions. The initial endothermic peak could be attributed to the removal or vaporization of extraneous materials. In contrast, the exothermic peak at 631.6 could be related to the AlN oxidation in the sample holder. Samples CTN-600 and CTNA-600 were sintered at 600°C, and the DTA heating beyond this temperature would cause a new reaction in the alloy system. The thermogram of sample CTN-600 is plotted together with CTNA-600 to compare their thermal behaviour under DTA heating. For CTN-600, a low-temperature exothermic peak is observed at the early stage of heating, and this is followed by a sizeable endothermic peak at about 511.5°C, which is conspicuously absent in sample CTNA-600. The behaviour in this region is shown to be in contrast to that of sample CTNA-600 with AlN addition. The double exothermic peaks observed on the thermograms at relatively higher temperatures (883.1, 883.7, 1048.3 and 1072°C) are peculiar to both alloys, and these correspond to changes in phases and possible recrystallization behaviour. Samples CTN-650 and CTNA-650 are also shown to exhibit thermal properties similar to CTN-600 and CTNA-600, respectively. The main observation regarding the alloys prepared at 650°C and 700°C is that there is a forward shift of the exothermic peaks, which may be linked to the initial higher sintering temperature, which could have cancelled out the reactions at 494 and 631.6°C observed for CTNA-600. A broad exothermic peak at 1055°C for CTNA-650 is related to a phase change in the material.

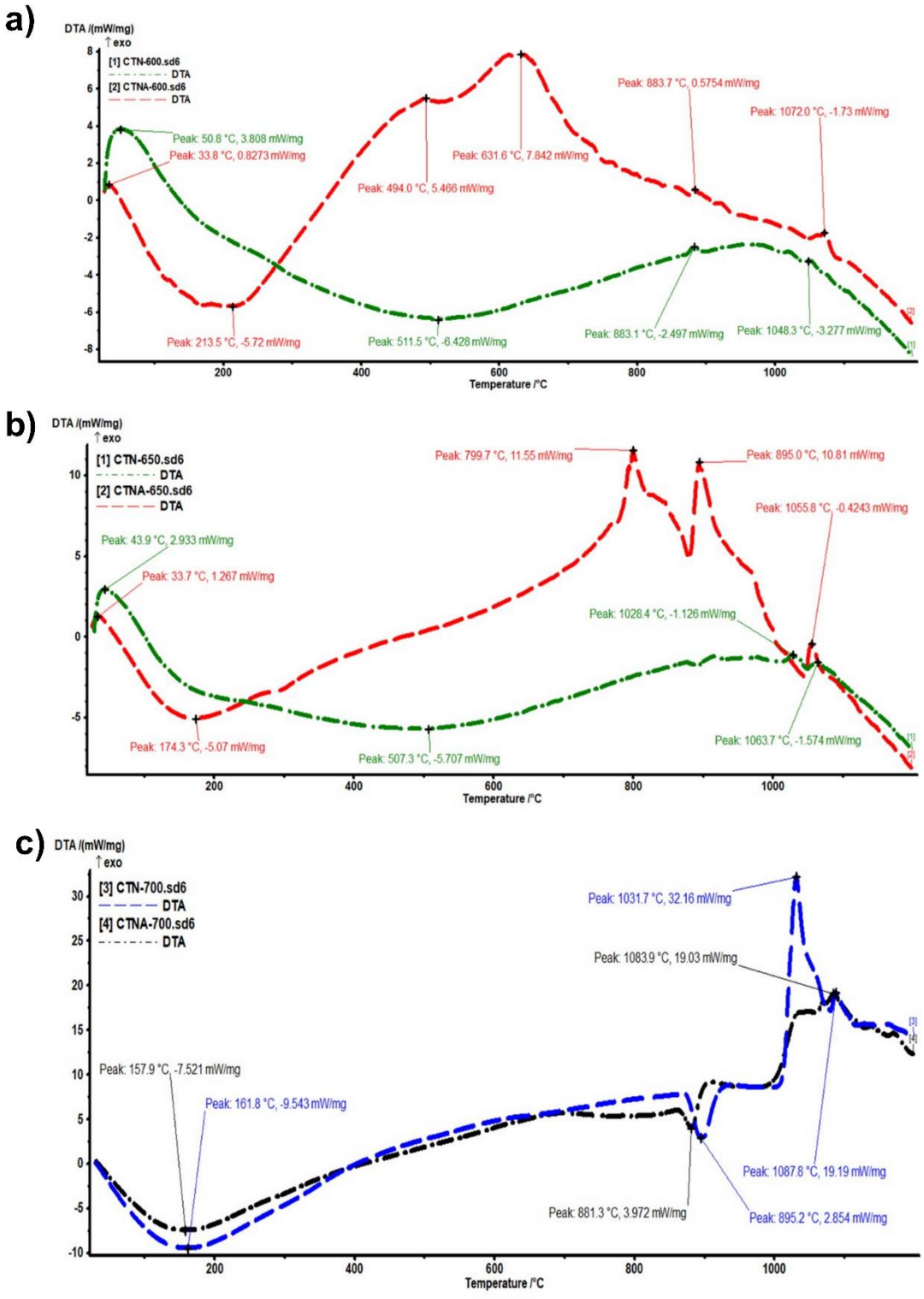

Figure 8 DTA thermograms for Cu alloy and metal matrix composite samples. **a)** DTA thermogram for samples CTN-600 and CTNA-600. **b)** DTA thermogram for samples CTN-650 and CTNA-650. **c)** DTA thermogram for samples CTN-700 and CTNA-700.

Meanwhile, for sample CTN-650, two successive low exothermic peaks are observed at 1028.4°C and 1063.7°C. These high-temperature peaks are due to oxidation and recrystallization of the metallic constituents of the alloy. The thermograms for samples CTN-700 and CTNA-700 also

indicate similarities in their thermal properties at higher temperatures. According to their thermograms, there is no observable presence of transformation reactions or a significant phase change till the endothermic peaks at 881.3 and 895.2°C for CTNA-700 and CTN-700, respectively. Afterwards, a sharp exothermic is observed for the pure ternary alloy sample, attributed to a significant phase change within the matrix. No central exothermic peak was observed for the sample CTNA-700 beyond 1000°C, and this shows good thermal stability of the alloys due to the presence of AlN during the initial heating reaction via plasma sintering. What is observed generally in all samples in terms of thermal analysis is the forward shift of the transformation or recrystallization reactions based on the sintering temperature(s), which might have caused primary reactions within the alloys at the initial stage.

The alloy samples were prepared at isothermal temperatures of 600, 650 and 700°C. However, the DTA experiment was done up to 1200°C. This means the samples were subjected to a temperature well beyond the sintering temperature. Thus, it provided the chance to learn about the thermal properties beyond the sintering isothermals. Notably, the Cu-Ti-Ni system has a ternary intermediate phase around the composition CuNiTi (Δ) that melts congruently at 1185°C, which is in perfect agreement with other studies [28]. Phases Δ have been found to form several pseudobinary eutectics with the intermediate phases, i.e., CuTi, NiTi, Ni3Ti binaries, and Cu and Ni [29, 30]. However, Gupta et al. [24] noted that the ternary phases found at 800 and 870°C are not observed at 600°C, except the Δ phase, which seems to be restricted to 600°C. Therefore, the exothermic and endothermic peaks observed at temperatures beyond the isothermal sintering temperature (600-700°C) can be attributed to the oxidation, formation and melting of phases due to the reactions with the alloy system.

3.4 Electrical Conductivity

Copper has the highest conductivity of any non-precious metal. This, combined with its high ductility, good machinability, and good corrosion resistance, makes copper the first choice as a conductor for electrical applications. However, its durability and strength in harsh environments are a concern for some high-end applications. Table 3 shows the values for the electrical properties of the sintered composites and alloys. It is observed that the sintering temperature and relative density remarkably influenced the electrical properties. Sample CTN-600 prepared without AlN nanoparticle possesses the lowest electrical conductivity. Meanwhile, sample CNTA-600 with aluminium nitride nanoparticle addition unexpectedly has higher electrical conductivity than CTN-600. The electrical conductivity value for CTNA-600 is comparable to those of samples prepared at higher sintering temperatures with an attendant higher compaction. The slight increase in the electrical conductivities at higher sintering temperatures can be attributed to the higher compaction of the constituents. Considering the effect of adding AlN nanoparticles on the copper matrix, it is observed that it has a negligible impact on conductivity.

Table 3 Electrical properties of sintered Cu12Ti(3-12)Ni - AlN alloys.

Sample	Sint. Temp. (°C)	ρ_{rel} (%)	ρ (μΩm)	σ (MS/m)
CNT-600	600	94.63	0.378	2.650
CNTA-600	600	88.96	0.195	5.130
CNT-650	650	95.59	0.180	5.560

CNTA-650	650	91.24	0.191	5.230
CNT-700	700	98.62	0.195	5.130
CNTA-700	700	95.58	0.164	6.080

Similarly, studies have shown that when the lattice orientation at the interface between the particles and matrix is coherent, the interface boundary effect on the electrical conductivity is negligible. In this case, the coherence could be attributed to the nano-size nature of the reinforcing particles, which might have improved coherence and enhanced compaction, thereby restricting grain boundary formation and aiding grain growth [31]. Based on the literature [32], the electrical conductivity of related Cu alloys, such as brass, bronze, CuNiSn, etc., is found in the range of 5 MS/m to 10 MS/m. These values are comparable to those obtained for the CuTiNi samples in the present work. Though these alloys (bronze, etc.) have relatively low electrical conductivity, their application areas require physical strength rather than high conductivity.

Furthermore, since the copper composites and alloys were prepared from powder constituents, a higher sintering temperature would enhance the thermal reaction between the particles. Thus the gaps within the grain would be drastically reduced. At lower sintering temperatures with lower Joule current flow, more gaps form within the matrix, obstructing the smooth flow of electrons for thermal and electrical conductivities. Hence, the observed nominal increase in the electrical conductivities with sintering temperatures is due to higher relative density. Notably, the Wiedemann-Franz Law relates the electrical and thermal conductivities of metals. Hence, it can be inferred that the same conditions also favour the thermal conductivity of the samples.

4. Conclusion

The influence of ceramic aluminium nitride nanoparticles on the microstructure and thermal and electrical properties of spark plasma sintered copper alloys have been studied successfully. The relative densities of the samples are shown to decrease with the addition of the ceramic reinforcement, which has the highest relative density attained by sample CTN-700 at 700°C. Meanwhile, the sample's microstructure is also observed to become more uniform and denser with sintering temperature. Changes in phase characteristics are observed with nitride addition, while the electrical and thermal conductivities increased monotonously with higher relative density through higher compaction and sintering temperature. The DTA indicate that the nitride nanoparticles conspicuously influence the thermal reaction of the alloy, recrystallization and phase transition activities observed in the higher temperature region of the thermograms for samples with aluminium nitride addition.

Acknowledgments

The authors wish to thank Tshwane University of Technology (TUT), Pretoria, South Africa., for the supports provided during this work. Also, the support of the National Research Foundation (NRF), South Africa is hereby acknowledged.

Author Contributions

Amos Oyatogun: Interpretation of results, sample preparation, manuscript preparation; Emmanuel Ajenifuja: Research supervision, sample preparation, manuscript preparation; Abimbola

Popoola: Project supervision, preliminary draft of procedure; Olawale Popoola: Project supervision, preliminary draft of procedure; Fatai Aramide: Specimen preparation and documentation; Grace Oyatogun: Preliminary draft of procedure, revision of preliminary reporting.

Competing Interests

The author has declared that no competing interests exist.

References

1. Guedes M, Ferreira JM, Rocha LA, Ferro AC. Vacuum infiltration of copper aluminate by liquid aluminium. Ceram Int. 2011; 37: 3631-3635.
2. Appendino P, Ferraris M, Casalegno V, Salvo M, Merola M, Grattarola M. Proposal for a new technique to join CFC composites to copper. J Nucl Mater. 2006; 348: 102-107.
3. Alvi S, Jarzabek DM, Kohan MG, Hedman D, Jenczyk P, Natile MM, et al. Synthesis and mechanical characterization of a CuMoTaWV high-entropy film by magnetron sputtering. ACS Appl Mater Interfaces. 2020; 12: 21070-21079.
4. Mofrad HE, Raygan S, Forghani BA, Hanaei K, Ahadi FK. Effect of cold-working and aging processes on the microstructure, mechanical properties and electrical conductivity of Cu-13.5% Mn-4% Ni-1.2% Ti alloy. Mater Des. 2012; 41: 182-191.
5. Soares AC, Ribeiro YD, Oliveira MP, de Azevedo MG, de Oliveira BF, Pereira AC, et al. Spark plasma sintered W, Ti_6Al_4V, Cu containing Nb-based alloys representing a new generation for high-temperature applications. J Mater Res Technol. 2022; 21: 2262-2276.
6. Olorundaisi E, Babalola BJ, Bayode BL, Teffo L, Olubambi PA. Optimization of process parameters for the development of Ni-Al-Ti-Mn-Co-Fe-Cr high entropy alloy system via spark plasma sintering. Int J Adv Manuf Technol. 2023; 126: 3323-3337.
7. Azzeddine H, Mehdi B, Hennet L, Thiaudière D, Alili B, Kawasaki M, et al. An in situ synchrotron X-ray diffraction study of precipitation kinetics in a severely deformed Cu-Ni-Si alloy. Mater Sci Eng A. 2014; 597: 288-294.
8. Zuhailawati H, Jamaludin SB. Studies on mechanical alloying of copper-tungsten carbide composite for spot welding electrode. J Mater Eng Perform. 2009; 18: 1258-1263.
9. Shichalin OO, Sakhnevich VN, Buravlev IY, Lembikov AO, Buravleva AA, Azon SA, et al. Synthesis of Ti-Cu multiphase alloy by spark plasma sintering: Mechanical and corrosion properties. Metals. 2022; 12: 1089.
10. Glibin VP, Kuznetsov BV, Vorobyova TN. Investigation of the thermodynamic properties of Cu-Ni alloys obtained by electrodeposition or by casting. J Alloys Compd. 2005; 386: 139-143.
11. Malekan M, Shabestari SG, Zhang W, Seyedein SH, Gholamipour R, Yubuta K, et al. Formation of bulk metallic glass in situ nanocomposite in $(Cu_{50}Zr_{43}Al_7)_{99}Si_1$ alloy. Mater Sci Eng A. 2012; 553: 10-13.
12. Sheng LY, Yang F, Xi TF, Lai C, Ye HQ. Influence of heat treatment on interface of Cu/Al bimetal composite fabricated by cold rolling. Compos B Eng. 2011; 42: 1468-1473.
13. Tayyebi M, Rahmatabadi D, Karimi A, Adhami M, Hashemi R. Investigation of annealing treatment on the interfacial and mechanical properties of Al5052/Cu multilayered composites subjected to ARB process. J Alloys Compd. 2021; 871: 159513.

14. Shao Y, Ding JT, Guo PY, Ou WX, Mao SY, Huang MR, et al. High temperature characteristics and phase compositions of Cu/Mn multilayers with the different average thickness prepared by electrodeposition. J Alloys Compd. 2021; 871: 159439.
15. Hilonga A, Kim JK, Sarawade PB, Kim HT. Rapid synthesis of homogeneous titania-silica composite with high-BET surface area. Powder Technol. 2010; 199: 284-288.
16. Florea RM. Understanding AlN obtaining through computational thermodynamics combined with experimental investigation. IOP Conf Ser Mater Sci Eng. 2017; 209: 012011.
17. Man GU, Wu YC, Jiao MH, Huang XM. Structural and mechanical properties of CuZr/AlN nanocomposites. Trans Nonferrous Met Soc China. 2014; 24: 380-384.
18. Gu M, Wu Y, Jiao M, Huang X. Structure and mechanical properties of Cu/AlN nano-composites with high strength and high conductivity. Rare Met Mater Eng. 2014; 43: 1562-1565.
19. Soffa WA, Laughlin DE. High-strength age hardening copper-titanium alloys: Redivivus. Prog Mater Sci. 2004; 49: 347-366.
20. El-Galy IM, Ahmed MH, Bassiouny BI. Characterization of functionally graded Al-SiCp metal matrix composites manufactured by centrifugal casting. Alexandria Eng J. 2017; 56: 371-381.
21. Miyamoto Y, Kaysser WA, Rabin BH, Kawasaki A, Ford RG. Functionally graded materials: Design, processing and applications. New York, NY: Springer; 1999.
22. Udupa G, Gangadharan KV. Future applications of carbon nanotube reinforced functionally graded composite materials. In: IEEE-international conference on advances in engineering, science and management (ICAESM-2012). Nagapattinam, India: IEEE; 2012. pp. 399-404.
23. Rubio WM, Paulino GH, Silva EC. Analysis, manufacture and characterization of Ni/Cu functionally graded structures. Mater Des. 2012; 41: 255-265.
24. Gupta KP. The Cu-Ni-Ti (copper-nickel-titanium) system. J Phase Equilib. 2002; 23: 541-547.
25. Gupta A, Talha M. Recent development in modeling and analysis of functionally graded materials and structures. Prog Aerosp Sci. 2015; 79: 1-14.
26. Yang D, Conrad H. Enhanced sintering rate of zirconia (3Y-TZP) by application of a small AC electric field. Scr Mater. 2010; 63: 328-331.
27. Yang D, Conrad H. Enhanced sintering rate and finer grain size in yttria-stablized zirconia (3Y-TZP) with combined DC electric field and increased heating rate. Mater Sci Eng A. 2011; 528: 1221-1225.
28. Gupta KP. Phase diagrams of ternary nickel alloys. Salt Lake, Kolkata: Indian Institute of Metals; 1990.
29. Alisova SP, Budberg PB, Koveneristyi YK. Liquidus surface in the Cu-TiNi-Ni systems. Ross Akad Nauk Met. 1992; 2: 223-226.
30. Alisova SP, Budberg PB, Koveneristyi YK. Phase transformation during solidification of Cu-Ni-Ti alloys with higher content. Ross Akad Nauk Met. 1992; 5: 218-223.
31. Feng J, Liang S, Song K, Guo X, Zhang Y, Li G, et al. Effects of particle characteristic parameters on the electrical conductivity of TiB_2/Cu composites: A modified model for predicting their electrical conductivity. J Mater Eng Perform. 2019; 28: 4316-4323.
32. Kuhn HA, Altenberger I, Käufler A, Hölzl H, Fünfer M. Properties of high performance alloys for electromechanical connectors. In: Copper alloys-early applications and current performance-enhancing processes. Norderstedt, Germany: Books on Demand; 2012. pp. 52-68.